Control of Ion Conduction in L-type Ca^{2+} Channels by the Concerted Action of S5–6 Regions

Susan M. Cibulsky and William A. Sather
Department of Pharmacology and Program in Neuroscience, University of Colorado Health Sciences Center, Denver, Colorado

ABSTRACT Voltage-gated L-type Ca^{2+} channels from cardiac (α_{1C}) and skeletal (α_{1S}) muscle differ from one another in ion selectivity and permeation properties, including unitary conductance. In 110 mM Ba^{2+}, unitary conductance of α_{1S} is approximately half that of α_{1C}. As a step toward understanding the mechanism of rapid ion flux through these highly selective ion channels, we used chimeras constructed between α_{1C} and α_{1S} to identify structural features responsible for the difference in conductance. Combined replacement of the four pore-lining P-loops in α_{1C} with P-loops from α_{1S} reduced unitary conductance to a value intermediate between those of the two parent channels. Combined replacement of four larger regions that include sequences flanking the P-loops (S5 and S6 segments along with the P-loop-containing linker between these segments (S5–6)) conferred α_{1S}-like conductance on α_{1C}. Likewise, substitution of the four S5–6 regions of α_{1C} into α_{1S} conferred α_{1C}-like conductance on α_{1S}. These results indicate that, comparing α_{1C} with α_{1S}, the differences in structure that are responsible for the difference in ion conduction are housed within the S5–6 regions. Moreover, the pattern of unitary conductance values obtained for chimeras in which a single P-loop or single S5–6 region was replaced suggest a concerted action of pore-lining regions in the control of ion conduction.

INTRODUCTION

The voltage-gated L-type Ca^{2+} channels from cardiac muscle (α_{1C}) and skeletal muscle (α_{1S}), though closely related in structure, differ from one another in a number of important functional ways. The high degree of sequence conservation between α_{1C} and α_{1S} has facilitated structure-function analysis for these channels. For example, structural elements regulating channel activation (Nakai et al., 1994) and mediating excitation-contraction coupling (Tanabe et al., 1990) have been identified using strategies that rely on this sequence similarity.

A substantial body of work has also been directed toward understanding the structural basis of ion selectivity in Ca^{2+} channels. Earlier work had led to the conclusion that selectivity in ion transport was mediated by preferential binding of Ca^{2+} over Na^+, the two principal competitors for transport through Ca^{2+} channels under physiological conditions (Almers and McCleskey, 1984; Hess and Tsien, 1984). More recent work using site-directed mutagenesis has identified amino acid residues that form the selectivity filter that binds Ca^{2+} in the pore (Tang et al., 1993; Yang et al., 1993; Ellinor et al., 1995; Cibulsky and Sather, 2000; Koch et al., 2000; Wu et al., 2000).

Despite the fact that tight binding of Ca^{2+} is essential for selection against nonpreferred permeants such as Na^+, the observed rate of Ca^{2+} conduction through the pore nonetheless requires fast Ca^{2+} unbinding and transit. For highly selective ion channels generally, no simple relationship between selectivity and conduction exists. Thus, for example, all voltage-gated K^+ channels are highly selective for K^+, yet their unitary conductance values range over two orders of magnitude (Hille, 2001). Likewise, voltage-gated Ca^{2+} channels are all highly selective for Ca^{2+}, and though less extreme than in the case of K^+ channels, different kinds of Ca^{2+} channels differ among themselves in unitary conductance. In particular, the unitary conductance of α_{1C} Ca^{2+} channels is roughly double that of α_{1S} channels.

Regions of Ca^{2+} channels that may be involved in specifying ion conduction include the P-loops, four pore-lining structures in each channel molecule that together contribute to formation of the selectivity filter. The P-loops are thought to line the extracellular portion of the pore in members of the voltage-gated ion channel family, which includes Ca^{2+} and K^+ channels (MacKinnon, 1995). Evidence provided by the crystal structure of a bacterial K^+ channel, an ancestor of both voltage-gated K^+ channels and Ca^{2+} channels, has strengthened this view (Doyle et al., 1998). This bacterial K^+ channel structure also shows that transmembrane segments homologous to S6 contribute to the intracellular portion of the pore, the portion that opens into the cytosol; the S6 segment appears to help form the intracellular portion of the pore in voltage-gated K^+ channels of higher organisms as well (del Camino et al., 2000). Consonant with this basic structural model, P-loops have been implicated in the control of unitary conductance in many members of the family of voltage-gated ion channels. In some cases, the P-loop or the entire S5–S6 linker that encompasses the P-loop has been suggested as the sole determinant of unitary conductance (Hartmann et al., 1991; Goulding et al., 1993; Yatani et al., 1994; Repunte et al., 1999). In other cases, flanking S5 and S6 segments were

Submitted June 27, 2002, and accepted for publication November 18, 2002.

Address reprint requests to William A. Sather, Department of Pharmacology, Box B-138, University of Colorado Health Sciences Center, 4200 East Ninth Avenue, Denver, CO 80262. Tel.: 303-315-3986; Fax: 303-315-2503; E-mail: william.sather@uchsc.edu.

S. M. Cibulsky's present address is Dept. of Neuroscience, Univ. of Pennsylvania, 223 Stemmler Hall, Philadelphia, PA 19104.

0006-3495/03/03/1709/11 $2.00

additionally shown to influence conduction (Aiyar et al., 1994; Shieh and Kirsch, 1994; Immke et al., 1998). Sequences even farther from the P-loop, including the cytosolically-disposed S4–S5 linker and C-terminal tail, have been implicated as determinants of unitary conductance (Isacoff et al., 1991; Slesinger et al., 1993; Choe et al., 2000). In the present work, we have used a systematic set of chimeras constructed between the α_{1C} and α_{1S} Ca^{2+} channel isoforms to identify domains that determine these channel's characteristic ion transport rates. The aim of work such as this is to understand how ion channels that are very similar in ion selectivity can differ significantly in rate of ion transport.

MATERIALS AND METHODS

Ca^{2+} channel chimeras

Three kinds of chimeras were constructed between cDNAs encoding the α_{1C} (Mikami et al., 1989; EMBL/GenBank accession number X15539) and α_{1S} (Tanabe et al., 1987; Kim et al., 1990; accession number X05921) L-type Ca^{2+} channel subunits. In the first kind of chimera, P-loop sequence was substituted from α_{1S} into α_{1C}. Based on the better-known structure of P-loops in voltage-gated K^+ channels (Yellen et al., 1991), P-loops of Ca^{2+} channels were, in this work, considered to be 18-residue sequences within the linker between the S5 and S6 transmembrane segments. However, in motif IV, 20-residue P-loop sequences were substituted to include one additional difference in sequence between the two parent channels. Numbering the EEEE locus glutamates as position 0 in each motif, the substituted P-loop regions comprised residue positions −13 to +4, amino to carboxy, or in the case of motif IV, positions −13 to +6. In α_{1S}, the P-loop segments for motifs I–IV were bounded by residues G279/D296, P601/S618, L1001/Q1018, and P1310/L1329; for α_{1C}, the P-loops were bounded by A380/D397, P723/S740, L1132/E1149, and P1433/M1452. In the other two kinds of chimeras, the entire sequence from the beginning of the S5 transmembrane segment through the end of the S6 segment (S5–6) was transferred from α_{1C} to α_{1S}, and vice versa. Hydropathy plot analysis has identified the S5 (20 residues) and S6 (25 residues) transmembrane segments in L-type Ca^{2+} channels (Tanabe et al., 1987), and the S5–6 regions of the four motifs range 100–136 residues in length. In α_{1S}, the S5–6 segments for motifs I–IV were bounded by residues I199/S334, L561/V661, I931/I1065, and V1270/M1384; for α_{1C}, the S5–6 segments were bounded by I301/S435, L684/V783, I1062/I1196, and V1393/M1506. The quadruple chimeras and the parent α_{1C} and α_{1S} subunits are diagrammed in Fig. 1. The single-motif chimeras for P-loop and S5–6 regions are not illustrated.

Chimeras were constructed using polymerase chain reaction (PCR) strategies. All PCR reactions were carried out using the Expand High Fidelity PCR kit (Boehringer-Mannheim, Indianapolis, IN). For construction of α_{1C}-based chimeras bearing P-loop sequence from α_{1S}, a four-primer strategy was used. Sense and antisense oligonucleotide fusion primers (primers 1 and 2; 51-mers) consisted of 32 bases of α_{1S} P-loop sequence flanked on one side by ~19 bases that were complementary to α_{1C} sequence. Single fusion primers did not span the entire P-loop sequence for a given motif, but their lengths were such that the 5′ ends (α_{1S} sequence) of sense and antisense fusion primers overlapped by 10 complementary bases. In two separate steps of PCR, either sense or antisense fusion primers were used in combination with a downstream or upstream flanking primer that was complementary to α_{1C} sequence (primers 3 and 4; 18mers). These reactions yielded a 5′ and a 3′ fusion fragment, which were then combined and allowed to anneal to one another by virtue of the 10-base complementary sequence. In a final PCR step, the annealed fragments were extended for five thermocycles, then the two flanking primers from the first rounds of PCR (primers 3 and 4) were added to the reaction mix, and the product was amplified in 15 additional thermocycles. The final PCR product and the vector bearing α_{1C} (pCARDHE) were subsequently digested with a pair of motif-specific restriction enzymes and gel-purified. Each P-loop chimera was completed by ligating the PCR cassette (396–659 bp, depending upon motif) into pCARDHE. α_{1C}-based chimeras bearing single P-loops from α_{1S} are referred to as $C_{IP}S$, $C_{IIP}S$, $C_{IIIP}S$, and $C_{IVP}S$; the subscripted Roman numeral indicates the motif within which the P-loop exchange was made. These individual P-loop chimeras were combined to produce an α_{1C}-based chimera in which all four P-loops were replaced by their counterparts in α_{1S}, and this construct is denoted $C_{QuadP}S$.

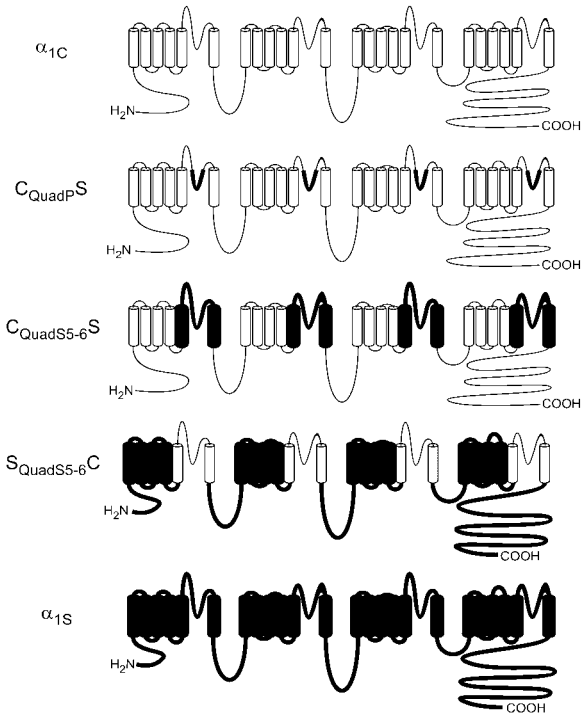

FIGURE 1 Schematic representation of the pore-forming subunits of wild-type α_{1C} and α_{1S} Ca^{2+} channels and some chimeric constructs. α_{1S} sequence is indicated by bold lines and by filled segments representing transmembrane regions, whereas α_{1C} sequence is indicated by thin lines and unfilled transmembrane segments. Only chimeras in which sequence was substituted in all four motifs are illustrated (Quad chimeras).

Chimeras in which S5–6 sequence from α_{1S} was substituted into α_{1C} are, for each of the four single-motif chimeras, denoted as $C_{IS5\text{–}6}S$, $C_{IIS5\text{–}6}S$, $C_{IIIS5\text{–}6}S$, and $C_{IVS5\text{–}6}S$. A four-motif chimera produced by combining the four S5–6 single-motif chimeras is referred to as $C_{QuadS5\text{–}6}S$. The S5–6 single-motif chimeras were constructed using a 5-primer strategy. In the first round of PCR, α_{1S} S5–6 sequence fused at either end to a short stretch of α_{1C} sequence was produced using an α_{1S} template and a pair of fusion primers (typically 39-mers; primers 1 and 2) that included 5′ overhangs (24 bases in length) corresponding to α_{1C} sequence located either immediately upstream of S5 or downstream of S6. In a second round of PCR, the gel-purified product of the first round, a primer complementary to upstream α_{1C} sequence (primer 3; 30-mer), primer 1, and an α_{1C} template were used to amplify the α_{1C} sequence upstream of S5. To avoid amplifying nonchimeric, WT α_{1C} in the final round of PCR, primer 3 included a 15-base, 5′-terminal, non-sense sequence that was complementary to neither α_{1C} nor α_{1S}. Primer 1 was added to this second-round reaction only after completing five thermocycles. In the third and final round of PCR, the gel-purified second-round product, a downstream primer complementary to α_{1C} sequence (primer 4; 18-mer), an upstream primer complementary to the nonsense sequence of primer 3 (primer 5; 15-mer), and α_{1C} template were used to amplify α_{1C} sequence downstream of S6. Primer 5 was added to the reaction

mix after completing five thermocycles. The final PCR product and the pCARDHE vector were digested with a pair of motif-specific restriction enzymes and gel purified. Each S5–6 chimera was completed by ligating the PCR cassette (600–1260 bp) into pCARDHE.

A chimera in which the S5–6 sequences of the four motifs of α_{1S} were replaced by the corresponding sequences in α_{1C} is referred to as $S_{QuadS5–6}C$. To make this chimera, the *Sac* II–*Bgl* II fragment of α_{1S}, corresponding to most of the coding region, was first subcloned into pGEMHE (Liman et al., 1992) to make use of advantageous restriction sites in this construct. The strategy used to construct the $S_{QuadS5–6}C$ chimera was conceptually similar to that described for the $C_{QuadS5–6}S$ chimera.

DNA sequences for all chimeras were confirmed by restriction digests and dideoxy chain termination sequencing of both strands of all PCR-amplified regions.

Ca^{2+} channel expression in *Xenopus* oocytes

cRNAs encoding α_1 subunits were synthesized using vectors for α_{1C}- and α_{1S}-based constructs that yielded high functional expression in *Xenopus* oocytes. Before construction of α_{1C}-based chimeras, the α_{1C} insert was subcloned into a modified version of pGEMHE, a vector that incorporates the 5′ and 3′ untranslated regions of the *Xenopus* β-globin gene (Liman et al., 1992). In the subcloning process, several in-frame start- and stop-codons in the 5′ untranslated region of the original α_{1C} clone were deleted, and a Kozak consensus sequence for initiation of translation was inserted immediately upstream of the true α_{1C} start codon. The resulting high-expression construct, termed pCARDHE, was used in the fabrication of all α_{1C}-based chimeras.

To enhance expression of α_{1S} in *Xenopus* oocytes, the 3′ coding region was truncated (Ren and Hall, 1997; Morrill and Cannon, 2000). One α_{1S} construct was truncated after the codon specifying amino acid 1662 (Beam et al., 1992) and another construct was truncated after codon 1698 (DeJongh et al., 1991; Ren and Hall, 1997). However, when subcloned into pGEMHE, neither the full-length α_{1S} cDNA nor the two 3′-truncated forms of α_{1S} yielded highly-expressed cRNAs (~100–500 nA whole-oocyte Ba^{2+} currents when coexpressed with $\alpha_2\delta_{1a}$ and β_{1b}). When subcloned into pAGA2 (Ren and Hall, 1997), the version of α_{1S} truncated after codon 1698 produced significantly larger currents. Therefore, after the $S_{QuadS5–6}C$ chimera was constructed in pGEMHE, the *Sac* II–*Bgl* II fragment of the chimera was subcloned into the pAGA2 vector to enhance chimera expression.

To further enhance functional expression of Ca^{2+} channels, cDNAs for the ancillary subunits $\alpha_2\delta_{1a}$ (rabbit; Mikami et al., 1989; the 3′ noncoding region was truncated), β_{2b} (rabbit; Hullin et al., 1992; EMBL/GenBank accession number X64298), and β_{1b} (rat; Pragnell et al., 1991; accession number X61394) were subcloned into the modified version of pGEMHE that was used for α_{1C}. Ca^{2+} channel subunit cRNAs were transcribed in vitro using the mMESSAGE mMACHINE T7 RNA synthesis kit (Ambion, Austin, TX). Equimolar concentrations of α_1-, $\alpha_2\delta$- and β-subunit cRNAs were injected into *Xenopus laevis* oocytes. α_{1C}- and α_{1C}-based chimeras were coexpressed with $\alpha_2\delta_{1a}$ and β_{2b}, whereas α_{1S}- and α_{1S}-based chimeras were coexpressed with $\alpha_2\delta_{1a}$ and β_{1b}, except where noted. According to the most recently proposed systematic nomenclature, the subunit makeup of these channels is written $Ca_v1.2a/\beta_{2b}/\alpha_2\delta_{1a}$ for α_{1C}-based channels, and $Ca_v1.1a/\beta_{1b}/\alpha_2\delta_{1a}$ for α_{1S}-based channels (Ertel et al., 2000). Oocytes were dissociated from ovarian tissue by shaking in a Ca^{2+}-free OR-2 solution (in mM: 82.5 NaCl, 2 KCl, 1 $MgCl_2$, 5 *n*-(2-hydroxyethyl)piperazine-*n*′-(2-ethanesulfonic acid) (HEPES), pH 7.5 with NaOH) containing 2 mg/ml collagenase B (Boehringer-Mannheim) for 60–90 min. Injected oocytes were incubated in ND-96 solution (in mM: 96 NaCl, 2 KCl, 1.8 $CaCl_2$, 1 $MgCl_2$, 5 HEPES, pH 7.6 with NaOH) supplemented with 2.5 mM sodium pyruvate (Sigma, St. Louis, MO), 100 U/ml penicillin (Sigma) and 0.1 mg/ml streptomycin (Sigma). Injected oocytes were maintained at 18°C, and were studied 3–14 days postinjection.

Two-electrode voltage clamp recording

Whole-oocyte currents were recorded as described previously (Sather et al., 1993). The bath was continuously perfused with a Cl^--free, nominally 40 mM Ba^{2+} solution (in mM: 40 $Ba(OH)_2$, 52 TEA-OH, 5 HEPES, pH 7.4 with methanesulfonic acid). Owing to precipitation, Ba^{2+} concentration was substantially lower than the nominal value, and was measured as ~10 mM (Williamson and Sather, 1999). To test the Mg^{2+} permeability of α_{1S} channels, 40 mM or 100 mM $Mg(OH)_2$ solutions were used (in mM: 40 $Mg(OH)_2$, 52 TEA-OH, 5 HEPES, pH 7.4 with methanesulfonic acid, or 100 mM $Mg(OH)_2$, 5 HEPES, pH 7.4 with methanesulfonic acid). Currents were measured with a model OC-725C amplifier (Warner Instruments), filtered at 500 Hz (4-pole Bessel filter, Warner Instruments) and sampled at 1 kHz. Data were acquired and analyzed using software custom-written in AxoBASIC (Axon Instruments, Foster City, CA). For voltage pulses of size P, peak currents were subtracted using the average of 10 pulses to $-P/4$. For the Cd^{2+} block experiments, a 1 mM $CdCl_2$ stock solution was diluted to a final concentration of 1 μM in the Ba^{2+} solution.

Single-channel recording

The vitelline membrane was manually stripped from an oocyte after soaking in a hyperosmotic solution (Sather et al., 1993). Single-channel currents were recorded in cell-attached patches while the stripped oocyte was bathed in a high K^+ solution that zeroed the membrane potential (in mM: 100 KCl, 10 HEPES, 10 ethylene glycol-bis(beta-aminoethyl ether)-*n*,*n*,*n*′,*n*′-tetraacetic acid) (EGTA), pH 7.4 with KOH). The L-type Ca^{2+} channel agonist FPL 64176 (RBI, Natick, MA) was included in the bath solution at a concentration of 2 μM to prolong channel openings. Pipettes were pulled from borosilicate glass (Warner Instruments, Hamden, CT), coated with Sylgard (Dow Corning, Midland, MI) and heat-polished. Pipettes typically had resistances of 25–40 MΩ when filled with the recording solution of (in mM) 110 $BaCl_2$, 10 HEPES (pH 7.4 with TEA-OH). Single-channel records were obtained using an Axopatch 200A amplifier (Axon Instruments, Foster City, CA). The amplifier's internal filter was set to 10 kHz and an external filter (8-pole Bessel filter, Frequency Devices, Haverhill, MA) was set to 2 kHz, yielding a −3 dB frequency for the cascaded filters of 1.96 kHz. The data were sampled at 10 kHz using a Digidata 1200A (Axon Instruments) A/D converter and Pulse software (HEKA, distributed by Instrutech Corp., Great Neck, NY). Single-channel current amplitudes were determined by cursor analysis of long-duration openings (Pulse, HEKA).

RESULTS

In two-electrode voltage-clamp recordings, channels containing α_1 subunits of predominantly α_{1S}-based or α_{1C}-based origin carried currents of roughly similar size, with peak inward currents of typically ~1–3 μA in the 40 mM Ba^{2+} solution. The resulting similarity of voltage clamp quality and of single-channel event frequency facilitated comparisons among channel constructs.

The chimeric constructs were designed to study ion permeation. However, as an indicator of the specificity in effect of the structural manipulations, we examined whether channel gating might have been altered in the chimeras. We found that wild-type and chimeric channels containing α_{1C}-based subunits exhibited the fast activation kinetics expected for α_{1C} channels, whereas channels containing α_{1S}-based subunits exhibited the slow activation kinetics characteristic of the skeletal muscle Ca^{2+} channel (Fig. 2 *A*) (Tanabe et al.,

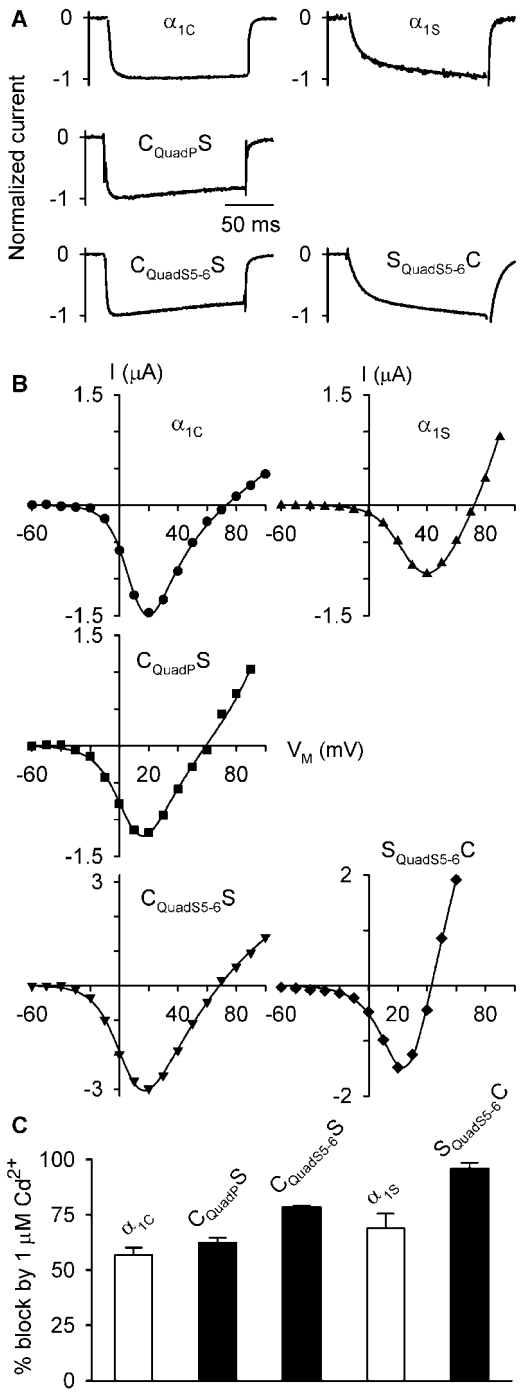

FIGURE 2 Whole-oocyte currents for α_{1C}, α_{1S}, and the three Quad chimeras ($C_{QuadP}S$, $C_{QuadS5-6}S$, and $S_{QuadS5-6}C$) with 40 mM Ba^{2+} solution in the bath. α_{1C} and α_{1C}-based chimeras were coexpressed with $\alpha_2\delta_{1a}$- and β_{2b}-subunits. α_{1S} and the α_{1S}-based chimera were coexpressed with $\alpha_2\delta_{1a}$- and β_{1b}-subunits. (*A*) Normalized currents elicited by test pulses to +20 mV. (*B*) Representative current-voltage relationships. Peak current is plotted versus test pulse voltage. Holding potential was −80 mV. (*C*) Percent block by 1 μM Cd^{2+} of inward Ba^{2+} current at +20 mV (mean ± SE; $n = 3$–10 oocytes).

1991). During a test pulse to +20 mV, τ_{act} for WT α_{1C} channels was 3.2 ± 0.1 ms (mean ± SE; $n = 6$), whereas τ_{act} for α_{1S} channels was 21.8 ± 1.0 ms ($n = 6$). The α_{1C}-based chimeras $C_{QuadP}S$ ($\tau_{act} = 2.4 \pm 0.3$ ms, $n = 6$) and $C_{QuadS5-6}S$ ($\tau_{act} = 1.3 \pm 0.1$ ms, $n = 6$) activated with time courses like that of wild-type α_{1C}, and the α_{1S}-based chimera $S_{QuadS5-6}C$ activated with a time course like that of α_{1S} (21.6 ± 3.7 ms, $n = 6$). Thus as judged by the general similarity of chimeras to their parents in regard to activation gating, these manipulations of pore structure appear to have had restricted effects on the behavior of the channels.

Selective permeability properties of wild-type and chimeric channels

In contrast to the lack of effect of altered pore structure on activation gating, indices of ion permeability were significantly affected by the structural alterations. Reversal potentials for whole-oocyte currents in 40 mM Ba^{2+} (Fig. 2 *B*) were modestly different between wild-type α_{1C} (E_{rev} = 73.2 ± 0.9 mV, $n = 12$) and α_{1S} ($E_{rev} = 67.7 \pm 1.0$ mV, n = 15). Each of the three quadruple chimeras exhibited reversal potentials that were less positive than for either of the wild-type channels, with $S_{QuadS5-6}C$ being the least selective for Ba^{2+} ($E_{rev} = 46.3 \pm 1.7$ mV, $n = 9$, for $S_{QuadS5-6}C$; 61.1 ± 2.1 mV, $n = 6$, for $C_{QuadP}S$; 63.9 ± 1.5 mV, $n = 8$, for $C_{QuadS5-6}S$). The fact that preference for Ba^{2+} over K^+ was reduced in all three chimeras relative to either parent channel suggests that interactions between the transferred sequences and the bulk of the channel protein were different from the corresponding interactions within the parent channels, with the implication that these specific interactions are important in the normal high selectivity of calcium channels. In addition, the observation that E_{rev} was reduced to a greater extent in the α_{1S}-based chimera than in the α_{1C}-based chimeras suggests that structural features specifying this measure of ion selectivity are different between α_{1C} and α_{1S}.

Percent block of Ba^{2+} current by 1 μM Cd^{2+} (Fig. 2 *C*) was also different between wild-type α_{1C} (56.9 ± 3.2%, n = 4) and α_{1S} (68.9 ± 6.7%, $n = 3$). Block of $C_{QuadP}S$ (62.4 ± 2.2%, $n = 10$) was intermediate between that of the two wild-type channels and block of $C_{QuadS5-6}S$ (78.4 ± 0.7%, $n = 6$) was somewhat greater than that of α_{1S}. $S_{QuadS5-6}C$, however, was significantly more sensitive to Cd^{2+} block than was either parent (96.0 ± 2.5%, $n = 6$). Based on the 1:1 binding that describes Cd^{2+} block of Ca^{2+} channels, these percent block values correspond to calculated half-block (IC_{50}) values of 757 nM and 451 nM for α_{1C} and α_{1S}; to 603 nM and 276 nM for the $C_{QuadP}S$ and $C_{QuadS5-6}S$ chimeras; and to 42 nM for the $S_{QuadS5-6}C$ chimera. Thus in all three cases, chimeric substitution increased the channel's affinity for Cd^{2+} relative to the parents. This systematic enhancement of Cd^{2+} affinity in chimeras relative to the parent channels suggests that, as for the reversal potential measurements, interactions between the transferred amino

acid sequence and the bulk of the channel protein are likely to be important in determining the structure and selectivity behavior of the pore.

Although Cd^{2+} block of Ba^{2+} current clearly differed between α_{1C} and α_{1S}, the differences were not so large that chimeras could be readily used to identify pore features responsible for differences in this property of the parent channels. And because Cd^{2+} sensitivity of the chimeras did not fall between that of the parents, Cd^{2+} block of Ba^{2+} current was not used for comparative structure-function analysis of α_{1C} and α_{1S} channels.

Previous work on native Ca^{2+} channels in skeletal muscle indicated that monovalent cation current carried by α_{1S} would be orders-of-magnitude less sensitive to block by Cd^{2+} than monovalent current carried by α_{1C} (compare Almers et al., 1984 with Yang et al., 1993), but we found no large difference between α_{1S} and α_{1C} in potency of Cd^{2+} block of monovalent current: Cd^{2+} blocked current carried by 100 mM Li^{+} through these two channels with roughly similar potency when the channels were expressed in oocytes (data not shown). It has also been reported that native skeletal muscle L-type Ca^{2+} channels can carry Mg^{2+} current (Almers and Palade, 1981; McCleskey and Almers, 1985), in contrast to the case for cardiac L-type channels (Hess et al., 1986; Lansman et al., 1986). For wild-type α_{1S} channels expressed in oocytes, however, we were unable to detect inward Mg^{2+} (40 mM or 100 mM) current. Thus because α_{1C} and α_{1S} differed only modestly or not at all in reversal potential, Cd^{2+} block, and Mg^{2+} permeability, we have focused our investigation of structural determinants of Ca^{2+} channel permeation upon the robust difference in unitary conductance between α_{1C} and α_{1S} channels, as described below.

Unitary conductance: P-loop transfer from α_{1S} to α_{1C}

Unitary current-voltage relationships in 110 mM Ba^{2+} for α_{1C} and α_{1S} are plotted in Fig. 3. The relationships for both wild-type channels as well as all of the chimeras are slightly curvilinear. They were, however, reasonably well fit with linear regressions. We used such fits to estimate unitary conductance (slope of the fit to data over the range −100 to +20 mV), which allows comparisons to be made with work by others. α_{1C} had a unitary conductance of 28.9 pS, which is in close agreement with the value of 29.1 pS measured from ventricular myocytes by Yue and Marban (1990). Conductance for α_{1S} was 16.3 pS, which is also similar to that measured from native channels, in this case, in skeletal myotubes (14.3 pS; Dirksen et al., 1997). The small difference between the two values for α_{1S} may be due to the difference in voltage range over which unitary current amplitude was measured: Dirksen et al. (1997) used −20 to +20 mV, whereas we used −100 to +20 mV, and curvature in the current-voltage relationship results in steepening of the

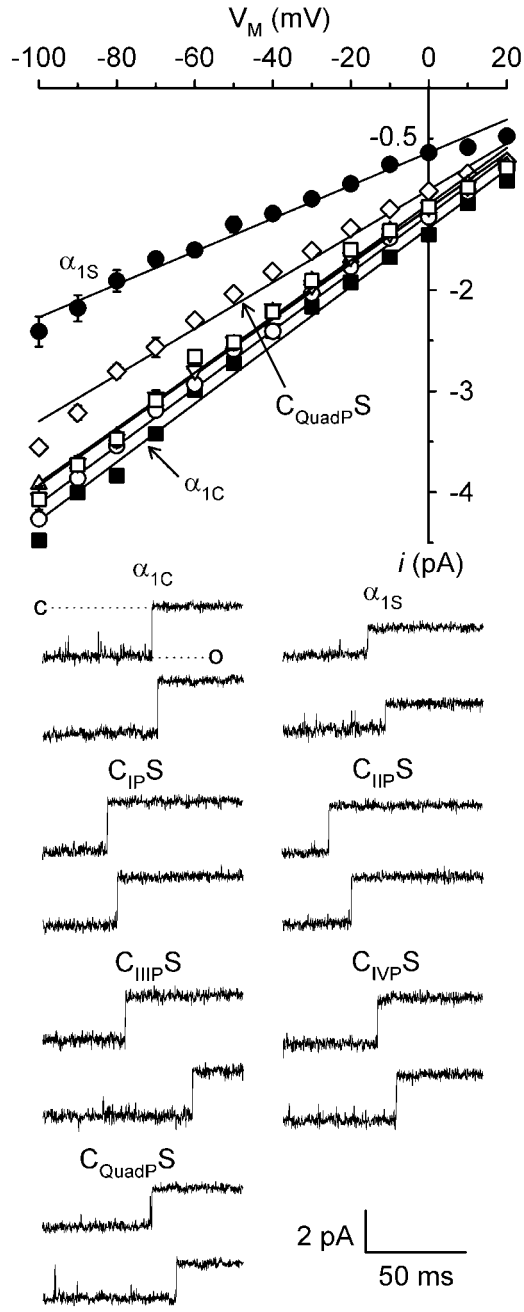

FIGURE 3 Unitary current-voltage relationships for α_{1C}, α_{1S}, and mutants in which P-loop sequence from α_{1S} was substituted into α_{1C}. α_{1C} and chimeras were coexpressed in oocytes with $\alpha_2\delta_{1a}$- and β_{2b}-subunits, whereas α_{1S} was coexpressed with $\alpha_2\delta_{1a}$- and β_{1b}-subunits. Currents in cell-attached patches were measured with 110 mM Ba^{2+} in the pipette. From the holding potential of −80 mV, a 25 or 50 ms prepulse of +20 to +80 mV was usually applied immediately before the 300 ms test pulse, with no interval between the prepulse and test pulse. The prepulse facilitated channel activation, and α_{1S} generally required stronger facilitation (+80 mV for 50 ms). Mean unitary current amplitude ± SE (n = 3–7 patches at each potential) is plotted versus test pulse voltage for α_{1S} (●), α_{1C} (■), $C_{IP}S$ (○), $C_{IIP}S$(△), $C_{IIIP}S$ (▽), $C_{IVP}S$ (□), and $C_{QuadP}S$ (◇). Solid lines represent linear regression fits to the data. Representative single-channel currents recorded during a test pulse to −40 mV are displayed in the lower part of the figure.

slope at more negative voltages. The transfers of P-loop sequences from α_{1S} to α_{1C}, one motif at a time, each had a small effect on unitary conductance (Fig. 3). P-loop replacement in motif II reduced α_{1C} conductance to 27.2 pS ($C_{IIP}S$), in motif III to 27.4 pS ($C_{IIIP}S$), in motif IV to 27.8 pS ($C_{IVP}S$), and in motif I to 28.6 pS ($C_{IP}S$). When all four P-loops were transferred together, conductance was reduced to a level intermediate between those for α_{1C} and α_{1S} ($C_{QuadP}S$; 22.9 pS). This observation, that replacement of all four α_{1C} P-loops with the corresponding α_{1S} P-loops did not fully transfer an α_{1S}-like conductance to α_{1C}, suggests that additional parts of the channel influence unitary conductance.

Unitary conductance: S5–6 transfer from α_{1S} to α_{1C}

For voltage-gated K^+ channels, evolutionary relatives of voltage-gated Ca^{2+} channels, structure-function studies have suggested that the cytoplasmic portion of the S6, and perhaps S5, transmembrane segments may line part of the inner pore (Choi et al., 1993; Aiyar et al., 1994; Lopez et al., 1994; Shieh and Kirsch, 1994; Taglialatela et al., 1994; Liu et al., 1997; del Camino et al., 2000). Structure-function studies have also implicated the intracellular loop between S4 and S5 in formation of the innermost part of the K^+ channel pore (Isacoff et al., 1991; Slesinger et al., 1993). In voltage-gated Ca^{2+} channels, evidence that S6 amino acids are critical for binding of pore-blocking phenylalkylamines indicates that S6 may form part of the inner pore in these channels as well (Streissnig et al., 1990; Hockerman et al., 1997). We therefore examined the role in ion conduction of the S5–6 region, which is composed of S5 and S6 segments and the entire sequence connecting S5 and S6, including the P-loop.

The size of the effect of transfer of S5–6 from α_{1S} to α_{1C} was motif-specific (Fig. 4). Replacement of S5–6 in motif I or in motif II had larger effects, lowering unitary conductance from the wild-type α_{1C} value of 28.9 pS to 24.4 pS in the $C_{IS5–6}S$ chimera or to 24.9 pS in the $C_{IIS5–6}S$ chimera. Transfer of S5–6 in either motif III or IV had almost negligible effect on unitary conductance (28.3 pS in $C_{IIIS5–6}S$ and 30.0 pS in $C_{IVS5–6}S$). The effect of single motif S5–6 transfers was in no case as large as the combined transfer of all four P-loops ($C_{QuadP}S$). However, replacement of all four S5–6 regions in α_{1C} produced a channel with an α_{1S}-like conductance: in fact, the conductance of $C_{QuadS5–6}S$ (14.1 pS) was slightly smaller than that of wild-type α_{1S} (16.3 pS). The similarity in conductance between wild-type α_{1S} and the $C_{QuadS5–6}S$ chimera suggests that, for wild-type α_{1C} versus wild-type α_{1S}, the differences in pore structure that are responsible for differences in unitary conductance are contained within the S5–6 regions.

Based on the results of previous work (Dirksen et al., 1997), our finding that the $C_{IS5–6}S$ chimera did not exhibit an α_{1S}-like conductance was unexpected. Dirksen and colleagues (1997) had found that the makeup of the region linking S5 with S6 in motif I, a sequence that formed part of the swapped region in our $C_{IS5–6}S$ chimera, was largely responsible for the difference in unitary conductance be-

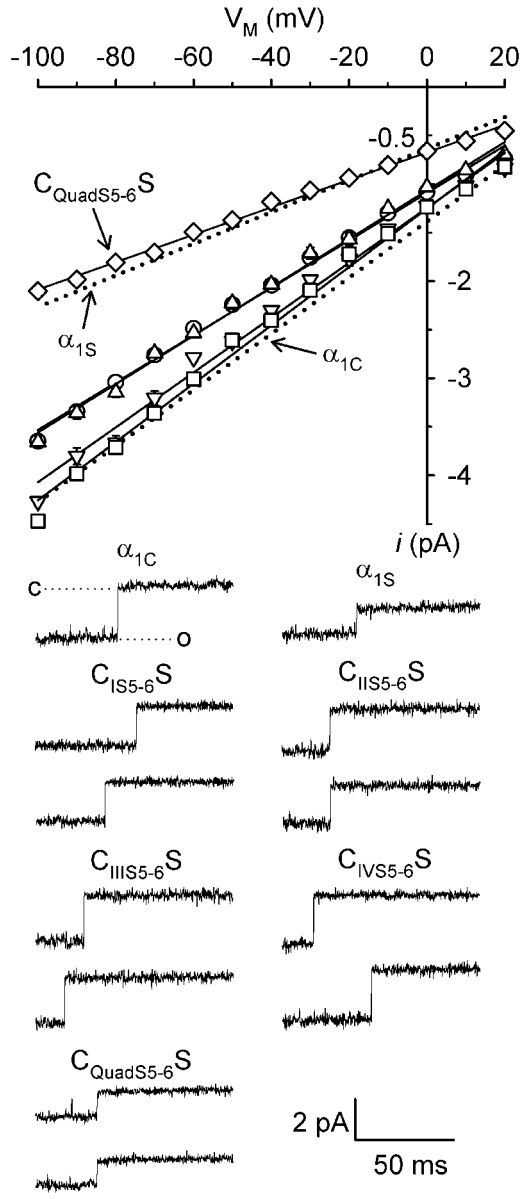

FIGURE 4 Unitary current-voltage relationships for chimeras in which S5 through S6 sequence from α_{1S} was substituted into α_{1C}. Chimeras were coexpressed in oocytes with $\alpha_2\delta_{1a}$- and β_{2b}-subunits. Currents in cell-attached patches were recorded with 110 mM Ba^{2+} in the pipette. Holding potential was −80 mV, and a 25 or 50 ms prepulse to +20 or +40 mV was usually applied to facilitate channel activation (no interval between prepulse in test pulse). Unitary current amplitude (mean ± SE, n = 3–7 patches at each potential) is plotted versus test potential for $C_{IS5–6}S$ (○), $C_{IIS5–6}S$ (△), $C_{IIIS5–6}S$ (▽), $C_{IVS5–6}S$ (□) and $C_{QuadS5–6}S$ (◇). Solid lines are linear regression fits to the data. For comparison, the linear regression fits to the i-V relationships for α_{1S} and α_{1C} from Fig. 3 are shown as dotted lines. Representative single-channel records at a test potential of −40 mV are illustrated in the lower part of the figure.

tween α_{1C} and α_{1S}. Among potential explanations for the contrasting findings, evidence that channel $\alpha_2\delta$- and β-subunits may influence unitary conductance (Meir and Dolphin, 1998) raised the possibility that our result with $C_{IS5-6}S$ might be attributable to its ancillary subunits. In the work reported here, we used a skeletal muscle $\alpha_2\delta$ isoform, similar to the experimental situation in the work by Dirksen and colleagues (1997). However, we used a β_{2b}-subunit in the work described above, in contrast to Dirksen and colleagues' reliance on the skeletal muscle β_{1a}- and β_{1b}-subunits (Ren and Hall, 1997). We therefore re-examined the unitary conductance of α_{1C} and α_{1C}-based chimeras, but with a skeletal muscle β-subunit coexpressed in place of β_{2b}. When coexpressed with β_{1b}, $C_{IS5-6}S$ had a unitary conductance (24.9 pS) that was little changed from its conductance when coexpressed with β_{2b} (24.4 pS). Nor was unitary current at -80 mV different when $C_{IS5-6}S$ was expressed with β_{1b} (-3.16 ± 0.03 pA, $n = 4$) versus β_{2b} (-3.04 ± 0.04 pA, $n = 5$). Unitary current amplitudes for $C_{QuadS5-6}S$ and wild-type α_{1C} were also unchanged by coexpression with β_{1b}. Thus under these conditions, β-subunit isoform does not appear to modulate the effects of transferred S5–6 sequences on unitary conductance.

Reciprocality of chimeric effects on unitary conductance: S5–6 transfer from α_{1C} to α_{1S}

The diminishment of unitary conductance produced by chimeric manipulation of the α_{1C} pore can be interpreted in competing ways. It might reflect the straightforward transfer of α_{1S}-like ion transport behavior along with α_{1S} pore sequence, or it might arise from incompatibility of the transferred α_{1S} sequence with the host α_{1C} sequence, resulting in misfolding in the pore region and retarded ion flux. To discriminate between these alternatives, we examined the unitary conductance of an α_{1S}-based chimera in which the four S5–6 regions were replaced with the corresponding sequences from α_{1C}. For this $S_{QuadS5-6}C$ chimera, complementary to $C_{QuadS5-6}S$, we specifically tested whether transfer of α_{1C} sequence into the α_{1S} host would yield a chimera with α_{1C}-like unitary conductance. Indeed, as illustrated in Fig. 5, the unitary conductance of the $S_{QuadS5-6}C$ (30.0 pS) chimera closely approximated that of the wild-type α_{1C} channel.

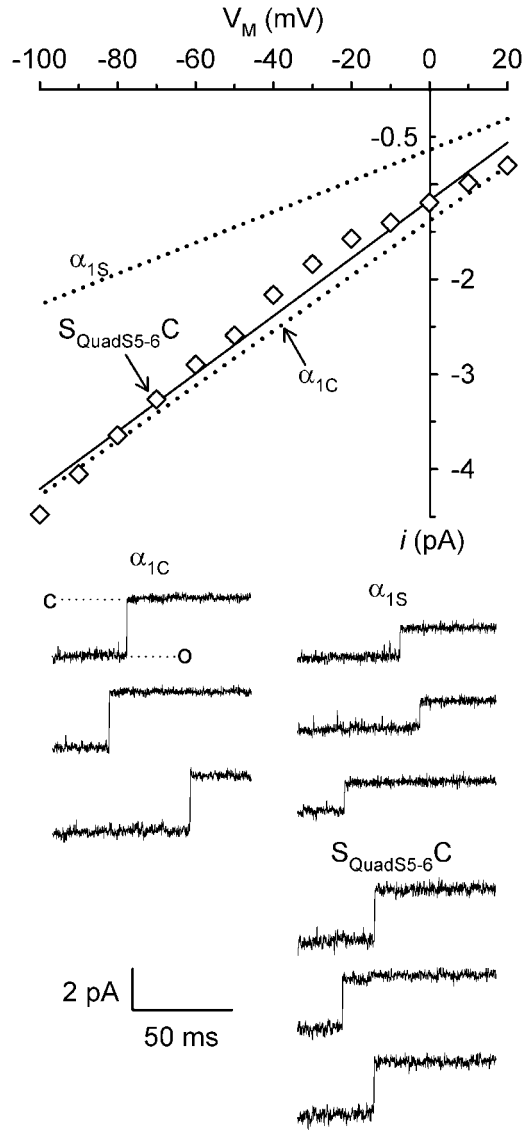

FIGURE 5 Unitary current-voltage relationship for the chimera in which S5 through S6 sequence from α_{1C} was substituted into α_{1S}, $S_{QuadS5-6}C$ (◇), (mean ± SE, $n = 3$–5 patches at each potential). The chimera was coexpressed in oocytes with $\alpha_2\delta_{1a}$- and β_{1b}-subunits. Currents were recorded in cell-attached patches with 110 mM Ba^{2+} in the pipette and with a holding potential of -80 mV. A 25- or 50-ms prepulse to $+20$ or $+40$ mV was given immediately before the test pulse to facilitate channel activation. The solid line is a linear regression fit to the data. For comparison, the linear regression fits to the *i*-V data for α_{1S} and α_{1C} are represented as dotted lines. Representative unitary currents recorded during a test pulse to -50 mV are illustrated below the *i*-V plot.

DISCUSSION

Our results provide evidence that the S5–6 regions, composed of transmembrane segment S5, the entire S5–S6 linker and transmembrane segment S6, contain the structural features that are responsible for the difference in unitary conductance between α_{1C} and α_{1S} L-type Ca^{2+} channels. The combination of the four P-loops, which represents a subset of the S5–6 regions, does not fully determine ion transport rate. Rather, the S5–6 regions from at least two motifs, and possibly all four, are required to specify the rate of ion transport through these channels. The reciprocal nature of the effects on ion conduction of the quadruple S5–6 swaps in α_{1C} and α_{1S} strengthens the conclusion that no other regions account for the characteristic ion transport rates of these L-channels.

S5–6 regions control ion flux through α_{1C} and α_{1S} Ca^{2+} channels

Unitary conductance and unitary current results for all the chimeras studied are compared in Fig. 6. The results are scaled relative to the normalized difference between α_{1C} and α_{1S} in either conductance (Fig. 6 *A*) or current (Fig. 6 *B*). Dotted lines mark values for α_{1C} (*upper level in both panels*) and α_{1S} (*lower level in both panels*). In general, the pattern of results is similar for unitary conductance and unitary current. Thus whether comparing conductance or current results for the quadruple chimeras (*black* or *white bars*), the quadruple P-loop substitution shifted the ion transport rate only about halfway toward the donor rate whereas quadruple S5–6 substitution more or less completely transferred the ion transport rate of the donor. Roles for non-P-loop regions in controlling ion conduction have previously been suggested for voltage-gated K^+ channels (Lopez et al., 1994; Aiyar et al., 1994; Shieh and Kirsch, 1994; Taglialatela et al., 1994; Immke et al., 1998) and for inward rectifier K^+ channels (Choe et al., 2000), and the full S5–6 region has been specifically implicated in cyclic nucleotide-gated channels (Siefert et al., 1999).

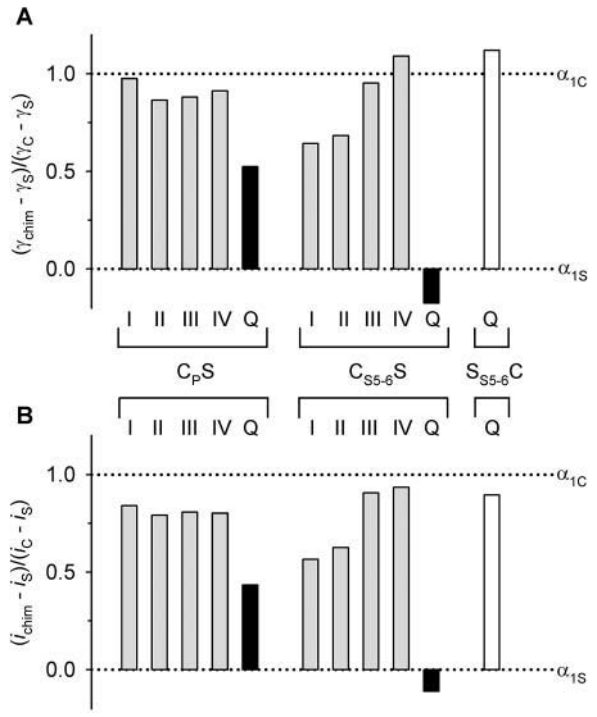

FIGURE 6 Summary of relative differences in unitary conductance (γ) and in unitary current (i) at −80 mV among α_{1C}, α_{1S}, and chimeras. (*A*) Differences in conductance between chimeras and α_{1S} ($\gamma_{chim} - \gamma_S$) are plotted relative to the difference in unitary conductance between α_{1C} and α_{1S} ($\gamma_C - \gamma_S$). Dotted lines represent the relative difference values for α_{1C} (1.0; $\gamma = 28.9$ pS) and α_{1S} (0; $\gamma = 16.3$ pS). For α_{1C}-based chimeras, bars representing single-motif substitutions (I, II, III, IV) are shaded in gray and bars representing Quad chimeras (Q; $C_{QuadP}S$ or $C_{QuadS5-6}S$) are filled in black. The α_{1S}-based Quad chimera (Q; $S_{QuadS5-6}C$) is represented by a white bar. Unitary conductance was determined from linear regression fits to unitary current amplitudes measured over the range −100 to +20 mV ($n = 3$–7 patches; 110 mM Ba^{2+}), as illustrated in Figs. 3–5. (*B*) Differences in unitary current at −80 mV between chimeras and α_{1S}, denoted ($i_{chim} - i_S$), are plotted relative to the difference in unitary current at −80 mV between α_{1C} and α_{1S}, denoted ($i_C - i_S$). Dotted lines represent the relative difference values for α_{1C} (1.0; $i = 3.83 \pm 0.03$ pA, $n = 4$) and α_{1S} (0; $i = 1.91 \pm 0.11$ pA, $n = 4$). For α_{1C}-based chimeras, bars representing single-motif substitutions (I, II, III, IV) are shaded in gray and bars representing Quad chimeras (Q; $C_{QuadP}S$ or $C_{QuadS5-6}S$) are filled in black. The α_{1S}-based Quad chimera (Q; $S_{QuadS5-6}C$) is represented by a white bar.

In comparing the results for individual motifs, three points emerge. First, different motifs are differentially important in determining ion transport rate. Although P-loop transfers produce roughly similar, small changes in ion transport rate, S5–6 transfers clearly are distinct from one another in the size of their effects. Thus among the S5–6 chimeras, transfer in motifs I and II produced the largest changes whereas transfer in motifs III and IV had lesser effects. Regarding the magnitude of effects produced by S5–6 substitution, the ordering of motifs is different for ion transport rate than it is for ion selectivity: for ion conduction, motifs I and II are most influential, whereas for ion selectivity, selectivity filter glutamate residues in motifs III and then II are most consequential (Yang et al., 1993; Ellinor et al., 1995). This contrast reiterates the point that ion conduction and selectivity are divergent phenomena in Ca^{2+} channels.

Second, the effects on conductance produced by single-motif sequence transfers are not in every instance additive: the magnitude of the change in ion transport rate produced by a quadruple transfer is not necessarily predicted by summing the magnitudes of the four corresponding single-motif transfers. In the most striking case, substituting all four α_{1S} S5–6 regions into α_{1C} ($C_{QuadS5-6}S$) reduced unitary conductance by about twice that of the summed reductions produced by the four individual S5–6 transfers. When considering instead unitary currents or the results for P-loops, the evidence for non-additivity was much weaker. Nonetheless, the absence of additivity of conductance for the S5–6 transfers raises the possibility of cooperative or synergistic interaction among the four motifs.

Third, interactions between P-loop sequence and other parts of the S5–6 region seem to be complex. The data summarized in Fig. 6 show that although individual S5–6 substitutions caused distinctive decrements in ion conduction, individual P-loop substitutions produced approximately similar, small decrements in ion conduction. Regarding motif IV, for example, P-loop substitution produced bigger changes in ion conduction than did S5–6 substitution, as though the effects of P-loop transfer could be reversed by transfer of structural features contained in the non-P-loop components of the S5–6 region. Alternatively, this finding might indicate that ''improper'' interactions of transplanted P-loop residues with host channel residues led to local protein misfolding and diminished ion conduction. This view may also account for our finding that Na^+ channel P-loops not only fail to confer Na^+ selectivity on Ca^{2+}

channels, but the resulting Na^+ channel/Ca^{2+} channel chimera also failed to carry Ca^{2+} or Ba^{2+} current (unpublished data).

Our findings generally agree with previous work by Dirksen et al. (1997) in that the motif I P-loop and S5–6 region house the key determinants of ion conduction, but our results using systematic sets of P-loop and S5–6 region chimeric constructs reveal significant participation of other motifs as well. In the study by Dirksen and colleagues (1997), substitution of α_{1S} sequence into the motif I S5–S6 linker of α_{1C}, which left the flanking S5 and S6 segments of α_{1C} in place, displaced unitary conductance ~75% of the way toward the α_{1S} value. In contrast, we have found that substitution of a larger region in motif I, encompassing the S5–S6 linker but also including the flanking S5 and S6 segments, displaced unitary conductance only ~35% ($C_{IS5–6}S$, Fig. 6 *A*) of the way toward the α_{1S} value. In our work, we found that full transfer of α_{1S}-like conductance required substitution of all four S5–6 regions. Various explanations for the apparent discrepancy between the two studies can be proposed, but a likely one stems from the fact that different chimeras were studied. As discussed above, interactions between the S5–S6 linker and surrounding parts of the S5–6 region may be important in determining conductance, and in the absence of appropriate interactions between these parts of the conductance-determining S5–6 regions, unitary conductance might consequently be reduced. The fact that swapping the four S5–6 regions reciprocally transferred unitary conductance between α_{1C} and α_{1S} confirms the idea that the S5–6 regions contain the structural features responsible for the difference in ion conduction between α_{1C} and α_{1S}. Comparison of results with our chimeras and those of Dirksen and colleagues (1997) also supports the idea, discussed above, that structural features contained within the S5–6 regions but outside the S5–S6 linker specify unitary conductance in these two L-type Ca^{2+} channels.

Reversal potential, Cd^{2+} block and unitary conductance

Whereas the unitary conductance results are interpretable in a straightforward manner, the effects of chimeric substitution on two other measures of ion permeability, reversal potential, and Cd^{2+} block, are not as readily rationalized. The parent α_{1C} and α_{1S} channels differed little from one another in E_{rev} and in estimated IC_{50} for Cd^{2+} block, but as a general trend, the three quadruple chimeras ($C_{QuadP}S$, $C_{QuadS5–6}S$, $S_{QuadS5–6}C$) differed from their parents: in the quadruple chimeras, E_{rev} was as much as 20 mV less positive ($S_{QuadS5–6}C$) and Cd^{2+} IC_{50} was as much as 10-fold lower ($S_{QuadS5–6}C$) relative to the parent channels. Thus quadruple chimerageneses seemingly reduced ion selectivity if judged from bi-ionic reversal potential, but increased ion selectivity if judged from Cd^{2+} binding affinity. The $S_{QuadS5–6}C$ chimera represents the most striking case, with the lowest preference for Ba^{2+} over K^+ (E_{rev}) but the highest preference for Cd^{2+} over Ba^{2+} (IC_{50}). Part of the explanation for this situation may be that these two measures of ion selectivity differ in the ions compared and in the direction of ion flow, so that inward Ba^{2+} competes with outward K^+ in one case but inward Cd^{2+} competes with inward Ba^{2+} in the other.

It is noteworthy that E_{rev} and IC_{50} were altered in the quadruple chimeras despite the fact that all four selectivity filter glutamates (EEEE locus) were present in these chimeras. One explanation is that the EEEE locus is very sensitive to structural context, so that incompatibility between α_{1C} and α_{1S} sequence in the chimeras results in altered EEEE locus configuration and altered selectivity. Alternatively, non-EEEE locus mutations have previously been found to affect Ca^{2+} channel selectivity, suggesting the possibility that altered pore structure elsewhere in the transplanted region might account for the changes in selectivity (Williamson and Sather, 1999; Feng et al., 2001).

Differences between α_{1C} and α_{1S} in S5–6 sequence and ion conduction

Sequence comparison suggests ways that the S5–6 regions might potentially control ion conduction in Ca^{2+} channels. In motif III, previous work comparing α_{1C} with α_{1A} (P/Q-type Ca^{2+} channel) sequence led to the finding that the side-chain volume of a residue neighboring the EEEE locus influenced unitary conductance (Williamson and Sather, 1999). The residue at this neighbor position is conserved between α_{1C} and α_{1S}, however, and in general, there are few remarkable differences in P-loop sequence between α_{1C} and α_{1S}, which may account for the inability of quadruple P-loop substitution to fully transfer conduction behavior. In the regions flanking the P-loops, the S5–S6 linkers differ between α_{1C} and α_{1S} at several positions. Examining these differences in motif I, α_{1C} has a net charge of -5 relative to α_{1S}, which has previously been suggested to attract permeant cations into the extracellular pore entrance and thereby impart higher conductance on α_{1C} channels (Dirksen et al., 1997). Considering this idea in light of the evidence that surrounding parts of S5–6 are important in specifying conduction rate, electrostatic enhancement of permeant ion entry rate may not be a dominant factor in conduction. Indeed, evidence against electrostatic focusing of permeant divalent metal cations at the mouth of L-type Ca^{2+} channels under the experimental conditions used here has been obtained (Kuo and Hess, 1992).

Regarding our evidence that the S5–6 region is crucial in controlling flux through Ca^{2+} channels, in the homologous K^+ channels the cytosolically-disposed part of S6 and possibly S5 is thought to contribute to the pore lining (Aiyar et al., 1994; Lopez et al., 1994; Shieh and Kirsch, 1994; Liu et al., 1997; Doyle et al., 1998; del Camino et al., 2000). The cytosolic halves of S5 and S6 in α_{1C} and α_{1S} are highly hydrophobic, which is consistent with the hydrophobicity of

homologous sequences lining the central pool and inner pore of the KcsA K^+ channel (Doyle et al., 1998). In Ca^{2+} channels, differences in these hydrophobic sequences may therefore help to determine conduction rate through the cytoplasmic part of the pore, as has been proposed for the KcsA channel. Additionally, the more extracellularly-disposed parts of the S5 and S6 segments may be involved, based on the fact that the number of differences in sequence between α_{1C} and α_{1S} is greater in the extracellular halves of S5 and S6 than in the intracellular halves. Whether amino acid residues in S5 or S6 contribute directly to pore formation in Ca^{2+} channels, for example at the extracellular entrance, is unknown. However, S5 and S6 may act by exerting indirect effects that influence the conformation of the more external portion of the pore, particularly the P-loop.

We thank Tsutomu Tanabe, Veit Flockerzi, Franz Hofmann, Kevin P. Campbell, and Linda M. Hall for gifts of Ca^{2+} channel cDNAs, and Emily Liman for the gift of the pGEMHE vector.

This work was supported by grant NS35245 (to W.A.S.) and fellowship MH11717 (to S.M.C.) from the National Institutes of Health.

REFERENCES

Aiyar, J., A. N. Nguyen, K. G. Chandy, and S. Grissmer. 1994. The P-region and S6 of Kv3.1 contribute to the formation of the ion conduction pathway. *Biophys. J.* 67:2261–2264.

Almers, W., and P. T. Palade. 1981. Slow calcium and potassium currents across frog muscle membrane: measurements with a vaseline-gap technique. *J. Physiol.* 312:159–176.

Almers, W., and E. W. McCleskey. 1984. Non-selective conductance in calcium channels of frog muscle: calcium selectivity in a single-file pore. *J. Physiol.* 353:585–608.

Almers, W., E. W. McCleskey, and P. T. Palade. 1984. A non-selective cation conductance in frog muscle membrane blocked by micromolar external calcium ions. *J. Physiol.* 353:565–583.

Beam, K. G., B. A. Adams, T. Niidome, S. Numa, and T. Tanabe. 1992. Function of a truncated dihydropyridine receptor as both voltage sensor and calcium channel. *Nature.* 360:169–171.

Choe, H., H. Sackin, and L. G. Palmer. 2000. Permeation properties of inward-rectifier potassium channels and their molecular determinants. *J. Gen. Physiol.* 115:391–404.

Choi, K. L., C. Mossman, J. Aube, and G. Yellen. 1993. The internal quaternary ammonium receptor site of *Shaker* potassium channels. *Neuron.* 10:533–541.

Cibulsky, S. M., and W. A. Sather. 2000. The EEEE locus is the sole high-affinity Ca^{2+} binding structure in the pore of a voltage-gated Ca^{2+} channel: block by Ca^{2+} entering from the intracellular pore entrance. *J. Gen. Physiol.* 116:349–362.

De Jongh, K. S., C. Warner, A. A. Colvin, and W. A. Catterall. 1991. Characterization of the two size forms of the alpha 1 subunit of skeletal muscle L-type calcium channels. *Proc. Natl. Acad. Sci. USA.* 88:10778–10782.

del Camino, D., M. Holmgren, Y. Liu, and G. Yellen. 2000. Blocker protection in the pore of a voltage-gated K^+ channel and its structural implications. *Nature.* 403:321–325.

Dirksen, R. T., J. Nakai, A. Gonzalez, K. Imoto, and K. G. Beam. 1997. The S5–S6 linker of repeat I is a critical determinant of L-type Ca^{2+} channel conductance. *Biophys. J.* 73:1402–1409.

Doyle, D. A., J. M. Cabral, R. A. Pfuetzner, A. Kuo, J. M. Gulbis, S. L. Cohen, B. T. Chait, and R. MacKinnon. 1998. The structure of the potassium channel: molecular basis of K^+ conduction and selectivity. *Science.* 280:69–77.

Ellinor, P. T., J. Yang, W. A. Sather, J. F. Zhang, and R. W. Tsien. 1995. Ca^{2+} channel selectivity at a single locus for high-affinity Ca^{2+} interactions. *Neuron.* 15:1121–1132.

Ertel, E. A., K. P. Campbell, M. M. Harpold, F. Hofmann, Y. Mori, E. Perez-Reyes, A. Schwartz, T. P. Snutch, T. Tanabe, L. Birnbaumer, R. W. Tsien, and W. A. Catterall. 2000. Nomenclature of voltage-gated calcium channels. *Neuron.* 25:533–535.

Feng, Z. P., J. Hamid, C. Doering, S. E. Jarvis, G. M. Bosey, E. Bourinet, T. P. Snutch, and G. W. Zamponi. 2001. Amino acid residues outside of the pore region contribute to N-type calcium channel permeation. *J. Biol. Chem.* 276:5726–5730.

Goulding, E. H., G. R. Tibbs, D. Liu, and S. A. Siegelbaum. 1993. Role of H5 domain in determining pore diameter and ion permeation through cyclic nucleotide-gated channels. *Nature.* 364:61–64.

Hartmann, H. A., G. E. Kirsch, J. A. Drewe, M. Taglialatela, R. H. Joho, and A. M. Brown. 1991. Exchange of conduction pathways between two related K^+ channels. *Science.* 251:942–944.

Hess, P., and R. W. Tsien. 1984. Mechanism of ion permeation through calcium channels. *Nature.* 309:453–456.

Hess, P., J. B. Lansman, and R. W. Tsien. 1986. Calcium channel selectivity for divalent and monovalent cations: voltage and concentration dependence of single-channel current in ventricular heart cells. 1986. *J. Gen. Physiol.* 88:293–319.

Hille, B. 2001. Ion Channels of Excitable Membranes. Sinauer Associates, Sunderland, MA.

Hockerman, G. H., B. D. Johnson, M. R. Abbott, T. Scheuer, and W. A. Catterall. 1997. Molecular determinants of high affinity phenylalkylamine block of L-type calcium channels in transmembrane segment IIIS6 and the pore region of the α_1 subunit. *J. Biol. Chem.* 272:18759–18765.

Hullin, R., D. Singer-Lahat, M. Freichel, M. Biel, N. Dascal, F. Hofmann, and V. Flockerzi. 1992. Calcium channel β-subunit heterogeneity: functional expression of cloned cDNA from heart, aorta and brain. *EMBO J.* 11:885–890.

Immke, D., L. Kiss, J. LoTurco, and S. J. Korn. 1998. Influence of non-P region domains on selectivity filter properties in voltage-gated K^+ channels. *Receptors Channels.* 6:179–188.

Isacoff, E. Y., Y. N. Jan, and L. Y. Jan. 1991. Putative receptor for the cytoplasmic inactivation gate in the *Shaker* K^+ channel. *Nature.* 353:86–90.

Kim, H. S., X. Y. Wei, P. Ruth, E. Perez-Reyes, V. Flockerzi, F. Hofmann, and L. Birnbaumer. 1990. Studies on the structural requirements for the activity of the skeletal muscle dihydropyridine receptor/slow Ca^{2+} channel. Allosteric regulation of dihydropyridine binding in the absence of α_2 and β components of the purified protein complex. *J. Biol. Chem.* 265:11858–11863.

Koch, S. E., I. Bodi, A. Schwartz, and G. Varadi. 2000. Architecture of Ca^{2+} channel pore-lining segments revealed by covalent modification of substituted cysteines. *J. Biol. Chem.* 275:34493–34500.

Kuo, C.-C., and P. Hess. 1992. A functional view of the entrances of L-type Ca^{2+} channels: estimates of the size and surface potential at the pore mouths. *Neuron.* 9:515–526.

Lansman, J. B., P. Hess, and R. W. Tsien. 1986. Blockade of current through single calcium channels by Cd^{2+}, Mg^{2+}, and Ca^{2+}: voltage and concentration dependence of calcium entry into the pore. *J. Gen. Physiol.* 88:321–347.

Liman, E. R., J. Tytgat, and P. Hess. 1992. Subunit stoichiometry of a mammalian K^+ channel determined by construction of multimeric cDNAs. *Neuron.* 9:861–871.

Liu, Y., M. Holmgren, M. E. Jurman, and G. Yellen. 1997. Gated access to the pore of a voltage-dependent K^+ channel. *Neuron.* 19:175–184.

Lopez, G. A., Y. N. Jan, and L. Y. Jan. 1994. Evidence that the S6 segment of the Shaker voltage-gated K^+ channel comprises part of the pore. *Nature.* 367:179–182.

MacKinnon, R. 1995. Pore loops: an emerging theme in ion channel structure. *Neuron*. 14:889–892.

McCleskey, E. W., and W. Almers. 1985. The Ca channel in skeletal muscle is a large pore. *Proc. Natl. Acad. Sci. USA*. 82:7149–7153.

Meir, A., and A. C. Dolphin. 1998. Known calcium channel α_1 subunits can form low threshold small conductance channels with similarities to native T-type channels. *Neuron*. 20:341–351.

Mikami, A., K. Imoto, T. Tanabe, T. Niidome, Y. Mori, H. Takeshima, S. Narumiya, and S. Numa. 1989. Primary structure and functional expression of the cardiac dihydropyridine-sensitive calcium channel. *Nature*. 340:230–233.

Morrill, J. A., and S. C. Cannon. 2000. COOH-terminal truncated $alpha_{1S}$ subunits conduct current better than full-length dihydropyridine receptors. *J. Gen. Physiol*. 116:341–348.

Nakai, J., B. A. Adams, K. Imoto, and K. G. Beam. 1994. Critical roles of the S3 segment and S3-S4 linker of repeat I in activation of L-type calcium channels. *Proc. Natl. Acad. Sci. USA*. 91:1014–1018.

Pragnell, M., J. Sakamoto, S. D. Jay, and K. P. Campbell. 1991. Cloning and tissue-specific expression of the brain calcium channel β-subunit. *FEBS Lett*. 291:253–258.

Ren, D., and L. M. Hall. 1997. Functional expression and characterization of skeletal muscle dihydropyridine receptors in *Xenopus* oocytes. *J. Biol. Chem*. 272:22393–22396.

Repunte, V. P., H. Nakamura, A. Fujita, Y. Horio, I. Findlay, L. Pott, and Y. Kurachi. 1999. Extracellular links in Kir subunits control the unitary conductance of SUR/Kir6.0 ion channels. *EMBO J*. 18:3317–3324.

Sather, W. A., T. Tanabe, J.-F. Zhang, Y. Mori, M. E. Adams, and R. W. Tsien. 1993. Distinctive biophysical and pharmacological properties of class A (BI) calcium channel α_1 subunits. *Neuron*. 11:291–303.

Siefert, R., E. Eismann, J. Ludwig, A. Baumann, and U. B. Kaupp. 1999. Molecular determinants of a Ca^{2+}-binding site in the pore of cyclic nucleotide-gated channels: S5/S6 segments control affinity of intrapore glutamates. *EMBO J*. 18:119–130.

Shieh, C.-C., and G. E. Kirsch. 1994. Mutational analysis of ion conduction and drug binding sites in the inner mouth of voltage-gated K^+ channels. *Biophys. J*. 67:2316–2325.

Slesinger, P. A., Y. N. Jan, and L. Y. Jan. 1993. The S4-S5 loop contributes to the ion-selective pore of potassium channels. *Neuron*. 11: 739–749.

Streissnig, J., H. Glossmann, and W. A. Catterall. 1990. Identification of a phenylalkylamine binding region within the a_1 subunit of skeletal muscle Ca^{2+} channels. *Proc. Natl. Acad. Sci. USA*. 87:9108–9112.

Taglialatela, M., M. S. Champagne, J. A. Drewe, and A. M. Brown. 1994. Comparison of H_5, S_6, and H_5-S_6 exchanges on pore properties of voltage-dependent K^+ channels. *J. Biol. Chem*. 269:13867–13873.

Tanabe, T., B. A. Adams, S. Numa, and K. G. Beam. 1991. Repeat I of the dihydropyridine receptor is critical in determining calcium channel activation kinetics. *Nature*. 352:800–803.

Tanabe, T., K. G. Beam, B. A. Adams, T. Niidome, and S. Numa. 1990. Regions of the skeletal muscle dihydropyridine receptor critical for excitation-contraction coupling. *Nature*. 346:567–569.

Tanabe, T., H. Takeshima, A. Mikami, V. Flockerzi, H. Takahashi, K. Kangawa, M. Kojima, H. Matsuo, T. Hirose, and S. Numa. 1987. Primary structure of the receptor for calcium channel blockers from skeletal muscle. *Nature*. 328:313–318.

Tang, S., G. Mikala, A. Bahinski, A. Yatani, G. Varadi, and A. Schwartz. 1993. Molecular localization of ion selectivity sites within the pore of a human L-type cardiac calcium channel. *J. Biol. Chem*. 268:13026–13029.

Williamson, A. V., and W. A. Sather. 1999. Nonglutamate pore residues in ion selection and conduction in voltage-gated Ca^{2+} channels. *Biophys. J*. 77:2575–2589.

Wu, X. S., H. D. Edwards, and W. A. Sather. 2000. Side chain orientation in the selectivity filter of a voltage-gated Ca^{2+} channel. *J. Biol. Chem*. 275:31778–31785.

Yang, J., P. T. Ellinor, W. A. Sather, J.-F. Zhang, and R. W. Tsien. 1993. Molecular determinants of Ca^{2+} selectivity and ion permeation in L-type Ca^{2+} channels. *Nature*. 366:158–161.

Yatani, A., A. Bahinski, M. Wakamori, S. Tang, Y. Mori, T. Kobayashi, and A. Schwartz. 1994. Alteration of channel characteristics by exchange of pore-forming regions between two structurally related Ca^{2+} channels. *Mol. Cell. Biochem*. 140:93–102.

Yellen, G., M. E. Jurman, T. Abramson, and R. MacKinnon. 1991. Mutations affecting internal TEA blockade identify the probable pore-forming region of a K^+ channel. *Science*. 251:939–942.

Yue, D. T., and E. Marban. 1990. Permeation in the dihydropyridine-sensitive calcium channel: multi-ion occupancy but no anomalous mole-fraction effect between Ba^{2+} and Ca^{2+}. *J. Gen. Physiol*. 95:911–939.